# Assessment of the performance of solar water heater: an experimental and theoretical investigation

Naseer T. Alwan[1,2,*], Milia H. Majeed[1], Ihsan M. Khudhur[3], S. E. Shcheklein[1], Obed M. Ali[3], Salam J. Yaqoob[4] and Reza Alayi[5,*]

*[1]Department of Nuclear and Renewable Energy, Ural Federal University named after the first President of Russia, B. N. Yeltsin 19 Mira St., Yekaterinburg 620002, Russia; [2]Power Mechanics Department, Technical Engineering College of Kirkuk, Northern Technical University, 36001 Kirkuk, Iraq; [3]Renewable Energy Research Unit, Northern Technical University, 36001 Kirkuk, Iraq; [4]Department of Research and Education, Authority of the Popular Crowd, Prime Minister, 10001 Baghdad, Iraq and; [5]Department of Mechanics, Germi Branch, Islamic Azad University, Germi, Iran*

## Abstract

This study aims to evaluate the performance of a flat plate solar water heater (SWH) theoretically and experimentally. The thermal performance of the SWH was predicted using Fortran 90 programming language. SWH was designed as a square shape with dimensions of 110 cm length, 120 cm width and 10 cm depth and tested by integrating with a modified solar distiller to increase the water temperature in the basin at a constant mass flow rate of 1.2 l/min. The tests were conducted under the weather condition of Yekaterinburg city, Russia, from June to September of 2019, and a typical day was chosen for each month (19 June, 17 July, 22 August and 15 September). The study revealed that the highest efficiency of the solar water collector obtained at the highest value of the intensity of solar radiation at mid-day. The maximum thermal efficiencies achieved on 17 July of 2019 were ∼67% and 66% based on theoretical and experimental analyses, respectively. A simultaneous increase in the water temperature and the intensity of solar radiation has been observed. During the four typical days of the experiment, the highest water temperatures of the solar collector were recorded during midday, i.e. 57.2°C, 64.4°C, 52.4°C and 49°C at the inlet, and 62.8°C, 71°C, 57.4°C and 53.2°C at the outlet for 19 June, 17 July, 22 August and 15 September 2019, respectively, while the solar radiation intensities recorded are 957, 1022, 840 and 723 W/m$^2$ for the test days.

*Keywords:* distillation; solar distiller; Fortran 90; thermal efficiency; solar water collector

*Corresponding author: nassir.towfeek79@gmail.com, reza.alayi@yahoo.com

Received 13 January 2022; revised 13 February 2022; accepted 28 February 2022

## 1 INTRODUCTION

Solar energy applications are considered one of the most critical solutions expected to face the problem of the sharp growth in global energy demand and mitigate the environmental impacts resulting from the use of fossil fuels [1–3]. Therefore, researchers sought to use solar energy effectively in domestic and industrial applications, such as solar water heating, one of the most promising applications in the water heating field [4]. Solar collectors are usually classified according to the design into non-concentrated and concentrated. The non-concentrated collectors include two types: the evacuated tubes and the flat plate type. [5].

Evacuated tube solar water collector consists of several closed glass tubes (a glass tube suspended inside a glass tube larger than it, the space between the tubes is filled with air, this air layer reduces heat loss from the solar water heater (SWH)), inside these glass tubes, high thermal conductivity copper tubes are installed; therefore, this type of solar heater has high thermal efficiency even on very cold days [6]. The flat plate solar collector consists of a galvanized plate, copper or stainless iron tubes, a glass cover and

International Journal of Low-Carbon Technologies 2022, 17, 528–539

https://doi.org/10.1093/ijlct/ctac032 Advance Access publication 19 April 2022

a thermally insulated structure. This type of SWH is characterized by high efficiency and ease of design and installation [7]. In the past 5 years, researchers have been striving to improve the performance of flat-panel and vacuum-tube solar heating systems. Sadeghi *et al.* [8] conducted an experimental study to improve the thermal properties of a vacuum tube-type solar water collector with different liquid volume flow rates (0.01, 0.03 and 0.05 ml/h) using copper oxide and water nano foil (Cu2O + W) with different concentrations, and a parabolic trough. The experiment's accuracy was verified by using artificial neural networks. Multilayer perceptron (MLP) and radial basis function methods were studied to predict the performance of a vacuum tube-type solar water collector. The results showed that the MLP model was more accurate. It was also observed that by increasing the flow rate and the concentration of the egocentric liquid, the thermal performance of the solar collector was increased. Muthuraman *et al.* [9] conducted an experimental study to improve the performance of the solar heater by adding design modifications including the use of spiral and curved copper tubes, according to the climatic conditions of Tamil Nadu/India. Several parameters of the solar heater were investigated, such as liquid mass flow rate inside the tubes, which were 0.0045 and 0.006 kg/sec. The results showed that the mass flow rate of 0.006 kg/sec recorded the highest thermal efficiency for straight, curved and spiral tubes about 62%, 65% and 73%, respectively. Also, the results show that the highest exergy efficiency was ∼32% for a mass flow rate of 0.0045 kg/s for the spiral tube solar water collector, and 27% for a mass flow rate of 0.006 kg/s for the spiral tube SWH.

The SWHs can directly be used in both industrial and domestic applications or as an auxiliary unit to supply hot water for systems like the solar water distiller to increase the temperature of its basin water [10, 11]. An effort to integrate water heater via glass evacuated pipes with a single basin still is reported by Sampathkumar *et al.* [12].

The anticipated procedure has augmented up to 72% of average daily production. A theoretical model was developed using governing energy equations. The theoretical results show agreement with the empirical results. The economic analysis of this scheme was indicated that the payback period will at 235 days.

Farahat *et al.* [13] designed and developed two conventional solar water stills integrating with flat plate solar water collectors and a thermal storage scheme. They are saving solar energy through daylight by the thermally insulated storage water tank. Two tests are studied. The first one has measured the production of the conventional solar still throughout daylight and night-time. Another still measuring the production by using recovered the solar energy both daylight and night-time. The recovered thermal with the assistance of forced circulation scheme and in the brackish water submerged a heat exchanger collected within the still basin. Therefore, the investigation for two stills with and without thermal recovery was presented. The results show that the daily output of still with thermal recovery system is twice as that of the conventional one. The modified still shows that the production in August, September, November and December is increased by 75%, 94%, 121% and 109%, respectively.

Mirmanto *et al.* [14] presented a study to enhance the productivity of single slope solar still by adding fins to the solar still basin. For this purpose, three solar stills were examined: the first is conventional type, the second with 10 fins and the third with 15 fins. The results showed that the productivity was improved by adding fins to the basin, the highest distillate water productivity was recorded with the 15-fin solar still ∼1.404 l/day, followed by the 10 fins solar still ∼1.264 l/day and the lowest without improvement (conventional solar still) ∼1.185 l/day.

Shah [15] designed a stepwise basin as a replacement for the flat basin to decrease the water film depth and increase the surface area. They used a sprinkler to maintain a uniform brackish water distribution in the basin. The gravel was used as a thermal material for heat storage and was still placed in the solar basin to enhance the evaporation process. The gravel absorbs more thermal energy. Moreover, a flat plate collector was used to increase the water temperature before entering the solar distiller. The glass temperature reached up to 65.8°C, and the maximum vapor temperature reached midday was 73°C. The average daily yield from the experimental results was 2.24 l/m$^2$, while the theoretical results were 3.78 l/m$^2$, and efficiency was 60%. The economic evaluation showed that the payback period is within 7 months.

Singh [16] conducted an experimental study on a solar still combined with an outer solar collector. This proposed design helped keep the system operating during periods of low sunlight. The proposed solar distiller yield increased ∼120%. Also, it is observed that the ambient conditions directly affect productivity, and overnight production amounted to 14% of the daily production.

Extending to the former work of Selimli *et al.* [17] enhanced the productivity by connecting the solar still pond with an evacuated tube of the solar collectors experimentally. The investigation has shown that 62.5% of the rate of purified freshwater was improved by coupling the solar still pond with the solar water collector (an evacuated pipes). Sethi and Dwivedi [18] carried out thermal efficiency and exergy analysis to calculate the thermal performance of the double slope solar distiller combined with the flat solar water collector. The exergy efficiency was increased from 0.26% to 1.34%, and the daily thermal efficiency of solar still increased from 13.55% to 31.07%.

Mousa *et al.* [19] tested a solar system to produce hot water and distilled water from brackish feed water. The water solar still integrated with the solar collector (evacuated tube type) used to heat a fluid that circulates in a closed loop by thermal-siphoning phenomena. The hot current fluid passes through a water bath giving its thermal energy and causing some of the water to evaporate. The generated vapor condenses on a slope glass cover and is collected as distillate water. Experimental results showed that the solar still could produce 0.15 l of distilled water/hr. An analysis of the results showed that the solar still cumulative output distillate water was enhanced. Water vapor condenses by cooling the inclined glass cover. Jojoba oil and water were used as thermal fluids. Water as a thermal fluid obtained better production. The feedwater salinity has a great effect on solar still productivity. This is recognized when the water of salinity ranging between 0.5 g/l

(tap water) to 25 g/l was tested, whereas high salinity of feed water decreases the productivity.

Previous studies, as reviewed above, have shown that the thermal performance of a solar water collector is hugely influenced by its design, operation and weather characteristics. It can be used in different applications (domestic and industrial) either directly or as an auxiliary system (hybrid system) to improve and raise the efficiency of the other systems, such as solar stills. However, more studies are needed to verify the performance of a flat solar collector in relatively cold climates (Russia), and the possibility of using the hot water produced from it in different applications (domestic and industrial) or using it as an auxiliary secondary cycle in other applications such as solar stills.

Therefore, the current work proposed a new design of a flat plate solar water collector consisting of 30 copper tubes and galvanized steel plate with a constant water flow rate and check

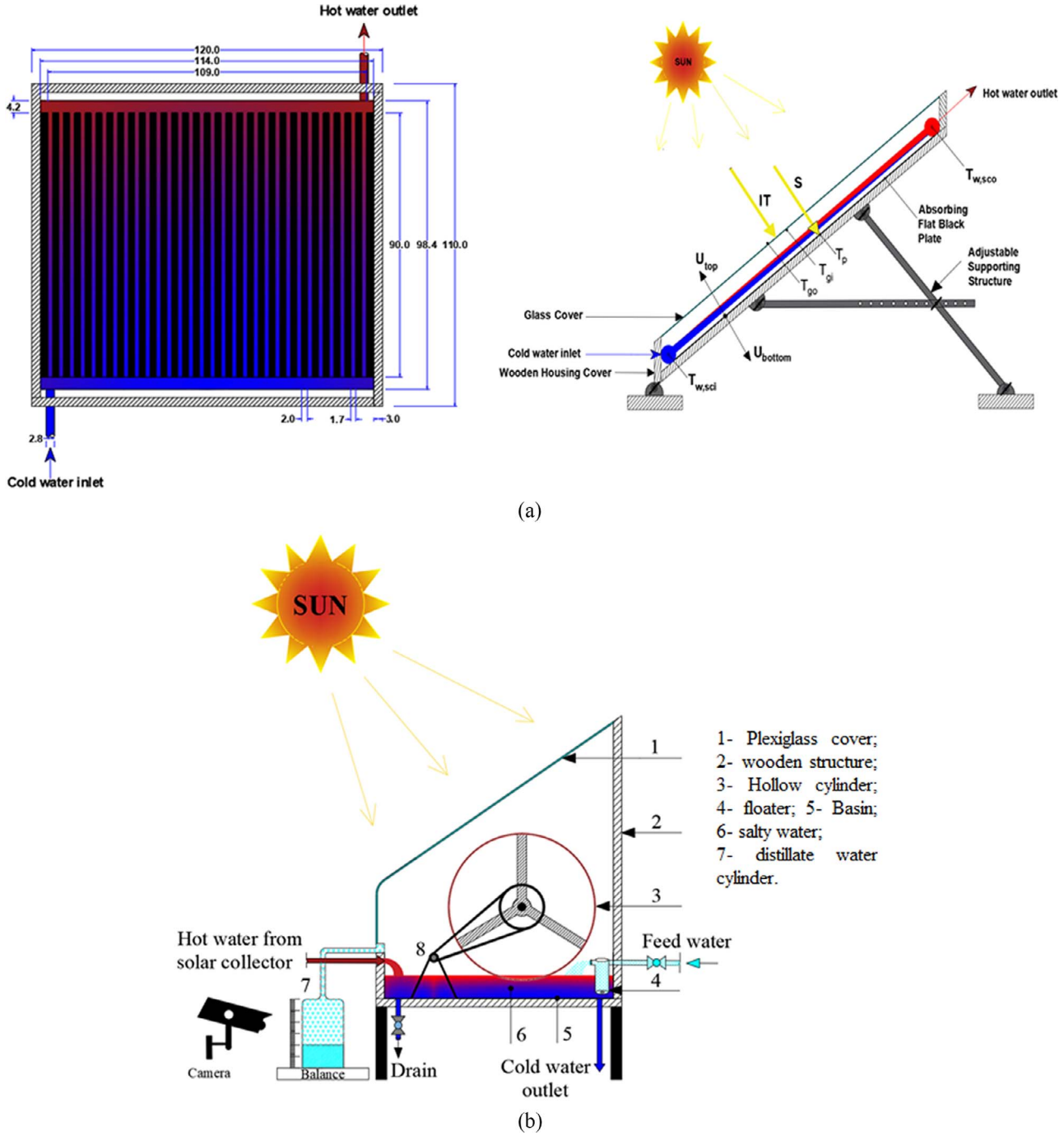


**Figure 1.** *Schematic diagram of (a) the solar water collector and (b) modified solar still.*

the thermal performance of this solar collector in relatively cold weather conditions (Russia) and showing the extent of its usefulness when used with different applications such as in the processes of additional heating of water basin in solar stills. This work included theoretical and experimental investigations of a flat-plate SWH combined with single slope solar still to increase the temperature of the solar still basin water under Yekaterinburg's weather conditions in Russia.

The study is presented as follows: the method is described in Section 2; Section 3 covers the theoretical analysis; and Section 4 covers the results and discussion. The conclusion for the study is provided in Section 5.

## 2 METHODOLOGY

During the process of solar water heating, the solar radiation that penetrates the glass cover is absorbed by the galvanized plate. Thus, it is heated, and the thermal energy is transferred to the copper tubes fixed on the surface of the plate and then to the working fluid (water). Therefore, the design and fabrication of solar water collectors is an important issue that should be considered carefully.

### 2.1 Description of the solar water collector understudy

Figures 1 and 2 show a diagram and photograph of the flat plate solar collector integrated with modified solar still (based on the use of a rotating hollow cylinder and integrated with an external solar water collector). Description of the solar water collector under study and the integration between this solar collector and the modified solar distiller has been mentioned in detail by Alwan et al. in the works [20].

### 2.2 Experimental method and uncertainty analysis

The current study included 40 tests under different environmental conditions from June to September of 2019, and a typical day was chosen for each month (19 June, 17 July, 22 August and 15 September). All the tests started at 8:00 am to 8:00 pm. The experimental setup was installed on the rooftop of the laboratory of the Department of Nuclear Power Plants and Renewable Energy Sources, Ural Federal University. To verify the performance of the solar collector under study, it was combined with the modified solar distiller [10]. The water was circulated between the two combined systems by a small pump with a constant flow rate of 1.2 l/min.

Parameters affecting the thermal performance of the solar collector were measured, including temperature values at different points of the solar collector as shown in Figure 3b, such as the glass cover ($T_{gi}$), absorber plate ($T_P$), water at the entrance and exit of the solar collector ($T_{s.ci}$ and $T_{s.co}$), the intensity of solar radiation and wind speed by different measuring devices [20].

In the experimental investigation, uncertainty analysis is an important step to give credibility to the results. To compute the uncertainty analysis resulting from practical measurements for each measuring instrument, first, one must know the accuracy values for each device used. Table 1 includes the values of accuracy and error ratio of measurement for each device. For the analysis of uncertainty, the following equations are used [21].


**Figure 2.** *Photograph view of the SWH integrated with the modified solar still.*

$$S' \text{ (standard deviation)} = \sqrt{\frac{\sum_{i=1}^{n} (X_i = X')^2}{n-1}} \quad (1)$$

$$S.E \text{ ( standard error)} = \frac{S'}{\sqrt{n}} \quad (2)$$

$$Error\% = \frac{S.E}{X'} * 100 \quad (3)$$

$$X' = \frac{\sum_{i=1}^{n} X_i}{n} \quad (4)$$

*where* $X_i$ *is the measured value,* $X'$ *is the mean measured value and n is the number of measurements recorded.*

According to studies [22, 23], it should take into account the regression uncertainties of the parameters of the calculations (indirect measurements) such as solar radiation; useful energy; thermal efficiency ($\eta_{s.c}$), which are a function of several operational parameters (direct measurements) such as the mass flow rate of water through the solar collector ($\dot{m}_w$); the heat capacity of water ($cp_w$); the temperature of the ambient air (Ta); and the temperature of the water at the inlet and the outlet of the solar collector ($T_{w,sci}$ and $T_{w,sco}$). It turns out that the estimated value of the average thermal efficiency conversion factor is affected by 1% when there is an uncertainty in I(t) ~1%. The useful energy is displaced by ±14.94% when the uncertainty of the temperature indicator is around ±1°C.

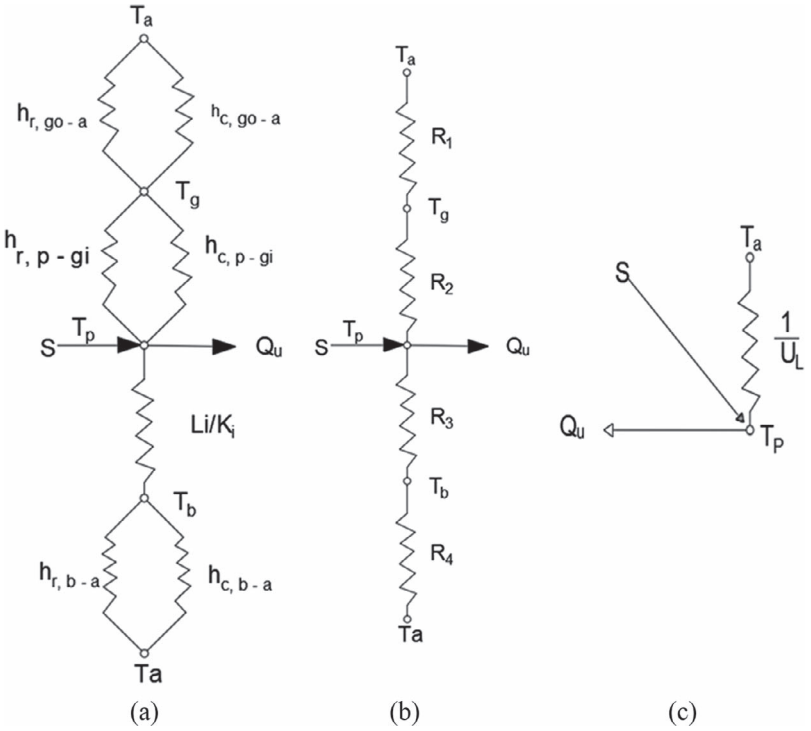


**Figure 3.** *Flat plate solar water collector thermal network (a) in the term's convection, conduction and radiation resistance; (b) in terms of resistances between surfaces; (c) equivalent thermal network [24].*

## 3 THEORETICAL ANALYSIS

The following assumptions are used to build the system model [24]:

1. steady state conditions;
2. the headers cover a small area of the collector and because of this can be neglected;
3. there is no heat absorption by the glass cover and the heat flow through it in one dimension;
4. the heat flow through the back insulation in one dimensional;
5. the impact of dust and dirt on the collector is minimal (it can be neglected).

To save time, reduce costs and avoid complex measurements, theoretical analysis was used in the present study. FORTRAN 90 programming language is used to carry out the theoretical calculations. To implement the theoretical model, the heat balance of the system was assumed.

### 3.1 Energy balance equations of the plate flat solar water collector

The useful energy $Q_u$ produced from a flat plate SWH at a steady-state condition is [24]:

$$Q_u = A_{s.c} * F_R * \left[S - U_L \left(T_{w,sci} - T_a\right)\right] \quad (5)$$

$$Q_u = \dot{m}_w * Cp_w * \left(T_{w,sco} - T_{w,sci}\right) \quad (6)$$

$$\eta_{s.c} = \frac{\dot{m}_w * cp_w * \left(T_{w,sco} - T_{w,sci}\right)}{I\,(t)} \quad (7)$$

where $A_{s.c}$ is the aperture area of the collector ($m^2$); $U_L(T_{w,sci} - T_a)$ is the heat transfer lost from the collector to the ambient area by convection, conduction and radiation; $T_{w,sco}$ is the temperature of outlet water from the solar collector (°C); $T_{w,sci}$ is the inlet water temperature to the collector (°C); $T_a$ is the ambient temperature (°C); $\dot{m}_w$ is the mass flow rate of water (kg/s) and $Cp_w$ is the specific heat of the water (kJ/kg.°C); $\eta_{s.c}$ is the solar collector thermal efficiency; and I(t) is the total solar radiation ($W/m^2$).

In solar collectors, the actual useful heat gain is usually associated with the maximum useful heat gain of the solar collector if all the collector surface is at the inlet water temperature. This quantity is called the heat removal factor $F_R$ [24].

$$F_R = \frac{\dot{m}_w * cp_w}{A_c * U_L}\left[1 - e^{\left(-\frac{A_{s.c} * U_L * F'}{\dot{m}_w * Cp_w}\right)}\right] \quad (8)$$

$$F' = \frac{U_{Lo}}{U_L} = \frac{1/U_L}{w\left[\frac{1}{U_L[d_o + (w - d_o).F]} + \frac{1}{C_c} + \frac{1}{\pi.d_i h_{fi}}\right]} \quad (9)$$

where $F'$ is the factor of solar collector efficiency, $U_{Lo}$ heat lost coefficient from water to ambient air, $U_L$ is the loss heat transfer

**Table 1.** *Accuracy and the error ratio of measuring devices.*

| Instrument | Accuracy | Range | Standard uncertainty | Error% |
|---|---|---|---|---|
| Solar power meter | $\pm 1\ W/m^2$ | $0-2000\ W/m^2$ | $\pm 0.5\ W/m^2$ | 1.5 |
| Temperature indicator | $\pm 1°C$ | $0–100°C$ | $\pm 0.57°C$ | 1.3 |
| Mercurial thermometer | 0.1°C | $0–60°C$ | $\pm 0.05°C$ | 0.5 |
| Flow meter | $\pm 1\ kg/s$ | 1–2 | 0.5 | 0.01 |
| Anemometer | 0.05 m/s | 0–30 m/s | ±0.05 m/s | 3 |

coefficient from the absorber plate to the ambient air, w is the distance between the tubes (m), F is the fin straight fins efficiency, $d_o$ is the outer diameter of the tube (m), $d_i$ is the inner diameter of the tube (m) and $C_c$ is the bond tube thermal conductivity ($\frac{W}{m.K}$).

Figure 3a and b shows the heat network of the input thermal energy (solar energy), thermal losses and useful heat gain of the solar collector. Figure 3c shows the heat transfer network to and from the solar collector, where the heat is transferred from the top and bottom of the solar collector (thermal energy loss) by convection and radiation to the ambient air. The thermal energy transferred from the absorber plate to the glass cover is equal to the thermal energy that is transferred from the glass cover to the ambient air [24].

$$Q_{\text{Loss top, P-gi}} = h_{C,\ \text{P-gi}}\left(T_P - T_{gi}\right) + \frac{\sigma\left(T_P^4 - T_{gi}^4\right)}{\frac{1}{\varepsilon_p} + \frac{1}{\varepsilon_{gi}} - 1} \quad (10)$$

where $h_{C,\,P-gi}$ is the convection heat transfer coefficient from the absorber plate to the glass cover. Usually, the free-convection heat transfer data are related to three dimensionless parameters: Nusselt number ($N_u$), Rayleigh number ($R_a$) and Prandtl number ($P_r$), which were obtained by the following equations:

$$N_u = \frac{h_{C,\ \text{P-gi}} * L}{K} \quad (11)$$

$$h_{C,\ \text{P-gi}} = \frac{N_u * K}{L} \quad (12)$$

$$R_a = \frac{g * \beta' * \Delta T * L^3}{\nu * \alpha'} \quad (13)$$

$$P_r = \frac{C_P * \mu}{K} = \frac{\nu}{\alpha} \quad (14)$$

where L is the distance between the absorber plate and glass cover (m), K is the air thermal conductivity (W/m.k), g is the gravitational constant ($m/s^2$), $\beta'$ is the volumetric coefficient of expansion (for an ideal gas, $\beta' = \frac{1}{T}$), $\Delta T$ is the temperature difference between absorber plate and glass cover (K), $\nu$ is the air kinematic viscosity ($m^2/s$) and $\alpha'$ is the air thermal diffusivity ($m^2/s$). For tilt angles from $0^\circ$ to $75^\circ$, the relationship between the Nusselt number and Rayleigh number as [24];

$$N_u = 1 + 1.44\left[1 - \frac{1708(\sin 1.8\beta)^{1.6}}{R_a * \cos\beta}\right]\left[1 - \frac{1708}{R_a * \cos\beta}\right]\left[\left(\frac{R_a * \cos\beta}{5830}\right)^{\frac{1}{3}} - 1\right] \quad (15)$$

The heat loss becomes

$$Q_{\text{Loss top, P-gi}} = \left(h_{C,\ \text{P-gi}} + h_{r,\ \text{P-gi}}\right)\left(T_P - T_{gi}\right) \quad (16)$$

where $h_{r,\ P-gi}$: the coefficient of heat transfer by radiation between the absorber plate and glass cover [25];

$$h_{r,\ \text{P-gi}} = \frac{\sigma\left(T_P^2 + T_{gi}^2\right)\left(T_P + T_{gi}\right)}{\frac{1}{\varepsilon_p} + \frac{1}{\varepsilon_{gi}} - 1} \quad (17)$$

where $\sigma$ is Stefan Boltzmann's constant ($5.67 * 10^{-8}\ W/m^2k^4$), $\varepsilon_p$ is the emittance of the plate equal to (0.23) and $\varepsilon_g$ refers to the emittance of the glass equal to (0.88). The thermal resistance $R_2$ is as follows:

$$R_2 = \frac{1}{h_{C,\ \text{P-gi}} + h_{r,\ \text{P-gi}}} \quad (18)$$

The thermal resistance between the outside glass cover and the ambient air has the same form of equation (18), but the coefficient heat transfer by convection $h_{C,\ go-a}$ in ($W/m^2.K$) is due to wind speed expressed as [26];

$$h_{C,\ \text{go-a}} = 2.8 + 3V_a \quad (19)$$

where $V_a$ is the wind velocity in (m/s).

The radiation resistance from the outer glass cover is expressed as the exchange of radiation between its surface and the sky at sky temperature ($T_{sky}$) as follows [27]:

$$h_{r,\ \text{go-sky}} = \sigma * \varepsilon_g * \left(T_{sky}^2 + T_{go}^2\right)\left(T_{sky} + T_{go}\right) \quad (20)$$

The accurate model of the sky temperature is [24]:

$$T_{sky} = T_a\left[\left(0.711 + 0.0056T_{dp} + 0.000073T_{dp}^2 + 0.013\cos(15t)\right)\right]^{1/4} \quad (21)$$

where $T_{sky}$ and $T_a$ are in (K), $T_{dp}$ is the dew point temperature (°C) and t is the time from midnight (hr).

The resistance to the surrounding $R_1$ is then given by

$$R_1 = \frac{1}{h_{C,\ go-a} + h_{r,\ go-sky}} \quad (22)$$

Therefore, the top heat loss coefficient from the collector to the ambient air is

$$U_{top} = \frac{1}{R_1 + R_2} \quad (23)$$

The energy loss from the bottom of the collector represents the resistance, $R_3$ and $R_4$, as shown in Figure 3b. $R_3$ represents the thermal resistance to heat flow by conduction through the insulation material and $R_4$ represents the thermal resistance of the convection and radiation from the thermal insulation to the ambient air, as shown by the following equations:

$$R_3 = \frac{L}{K_{ins}} \quad (24)$$

where L is the thickness of wooden insulation (0.03 m) and $K_{ins}$ is the thermal conductivity of the insulation (W/m.K).

$$R_4 = \frac{L}{h_{C,b-a} + h_{r,b-sky}} \quad (25)$$

where $h_{c,\ b-a}$ is the convection heat transfer coefficient ($W/m^2/K$) to the environment is expressed as [26]:

$$h_{C,\ b-a} = 2.8 + 3 * V_a \quad (26)$$

where $V_a$ is the wind velocity (m/s).

$h_{r,\ b-sky}$ is the heat transfer coefficient by radiation can be written as

$$h_{r,\ b-sky} = \sigma * \varepsilon_b * \left(T_b^2 + T_{sky}^2\right)\left(T_b + T_{sky}\right) \quad (27)$$

$\varepsilon_b$ is the emittance of the bottom.

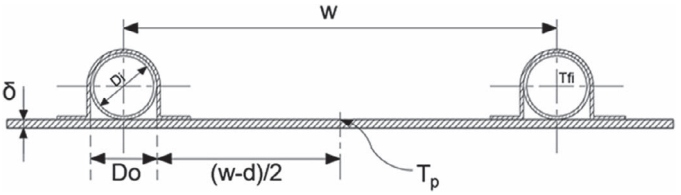


**Figure 4.** *The absorbed plate and tube dimension [24].*

Therefore, the total bottom loss coefficient from the collector to the ambient air is

$$U_{bottom} = \frac{1}{R_3 + R_4} \quad (28)$$

Edge losses are calculated by assuming 1D lateral heat flux around the perimeter of the collector. Losses should be indicated by the edge to the collector area. If the edge loss modulus area product is the $(UA)_{edge}$, so the edge loss coefficient, based on the collector surface area $A_{s.c}$ is

$$U_{edge} = \frac{(UA)_{edge}}{A_{s.c}} \quad (29)$$

So, the coefficient of overall thermal loss of $U_L$ is given by the following equation:

$$U_L = U_{top} + U_{bottom} + U_{edge} \quad (30)$$

Figure 4 shows the absorber plate and tube formation. The fin efficiency of the straight fins F is expressed as follows [24]:

$$F = \frac{\tanh\left[m\left(\frac{w-D_o}{2}\right]\right.}{m\left(\frac{w-D_o}{2}\right)} \quad (31)$$

where $m = \sqrt{\frac{U_L}{K*\delta}}$ (32).The absorber plate in study has a thickness $\delta$ = 1 mm, k the absorbed plate thermal conductivity (W/m.K) and temperature gradient through the absorbed plate is negligible. The tube is made of copper that is attached to the absorber plate by fixing clamps. The clamps conductance Cc was supposed to have a very large value; therefore, (1/Cc = 0). The $h_{fi}$ is the coefficient of heat transfer between the water and the tube wall. The water flow inside the tube is laminar because $Re_d$ = 202.5 [24]. Therefore, $h_{fi}$ can be calculated as follows [27]:

$$\overline{Nu}_d = \frac{h_{fi} * D_i}{K} = 4.36 \quad (33)$$

$$S = I_T * (\tau\alpha) \quad (34)$$

where $S$ is incident total solar energy (W/m$^2$), $(\tau.\alpha)$ = transmittance–absorption product and $I_T$ is the total solar radiation (W/m$^2$).

## 3.2 Hourly solar radiation

Hourly solar radiation intensity records are available for horizontal surfaces for many locations in the world. However, the solar radiation intensity records on inclined surfaces are generally not available. The first step to calculating the intensity of solar radiation at an inclined surface is to break down the horizontal solar radiation results of the beam rays and the diffuse rays. This is accomplished using the correlation by Tarik *et al.* [28], which relates ($I_d$/I) with the clearness index $k_T$. The correlation is

$$\frac{I_d}{I} = \begin{cases} 1 - 0.09 * K_T & K_T \leq 0.22 \\ 0.9511 - 0.16 * K_T + 4.388 * (K_T)^2 - \\ 16.638 * (K_T)^3 + 2.336 * (K_T)^4 & 0.22 < K_T \leq 0.8 \\ 0.165 & K_T > 0.8 \end{cases} \tag{35}$$

where $I_d$ is the diffuse radiation, I is the incoming solar radiation on the horizontal surface and the value $k_T$ is taken [29, 30] and where

$$K_T = \frac{I}{I_{ex}} \tag{36}$$

and $I_{ex}$ is extraterrestrial radiation at the horizontal surface for an hour, $I_{ex}$ in joule per square meter can be calculated by [24] as

$$I_{ex} = \frac{12 * 3600}{\pi} * G_{sco} * \left[1 + 0.033 \cos\left(\frac{360 * n}{365}\right)\right] * \left[\cos\varphi * \cos\delta * (\sin\omega_2 - \sin\omega_1) + \frac{2\pi\,(\omega_2 - \omega_1)}{360} * \sin\varphi \sin\delta\right] \tag{37}$$

However, the difference in distance between the earth and the sun changes the flow of radiation outside the Earth by about ±0.033.

$$G_{sco} = G_{sc}\big(1.00110 + 0.034221\cos B + 0.001280\sin B + 0.000719\cos 2B + 0.000077\sin 2B\big) \tag{38}$$

where $G_{sco}$ is the intensity of extraterrestrial radiation at the natural level of radiation per day $n^{th}$ of the year, and B is given by

$$B = (n - 1)\frac{360}{365} \tag{39}$$

where $G_{sc}$ is the solar constant (1367 W/m$^2$), δ declination (radian), n represents the day of the year, φ is the latitude angular (56.84°N), $\omega_2$ is the hourly angle at the end hour and $\omega_1$ is the hourly angle at the beginning hour:

$$\omega_1 = 15\,(i - 12) \tag{40}$$

$$\omega_2 = \omega_1 + 15 \tag{41}$$

where i is the hour of the day (i = 1…., 24). An approximate value for the sun's declination is calculated as follows [31]:

$$\delta = 23.45 * \sin\left(\frac{360\,(284 + n)}{365}\right) \tag{42}$$

The diffuse component ($I_d$) can be estimated from Erb's correlation, then the beam component ($I_B$) can be calculated by

$$I_B = I - I_d \tag{43}$$

The next step is to calculate the solar radiation per hour on the inclined surface $I_T$ as follows [32]:

$$I_T = R * I \tag{44}$$

where (R) is the ratio between the solar radiation on an inclined surface to the solar radiation on a horizontal surface. The sunray has three components: the beam, the diffuse through the sky and the diffuse on the ground surfaces—reflected rays. Assuming diffuse radiation to be isotropic, i.e. uniformly distributed over the skydome, R can be expressed by [24]:

$$R = \left(1 - \frac{I_d}{I}\right) * R_B + \frac{I_d}{I} * \frac{(1 + \cos\beta)}{2} + \rho_g + \frac{(1 + \cos\beta)}{2} \tag{45}$$

where β is the surface tilt angle

$$R_B = \frac{\cos\theta}{\cos\theta_z} \tag{46}$$

where

$$\cos\theta = \cos\delta * \cos(\varphi - \beta) * \cos\omega + \sin\delta * \sin(\varphi - \beta) \tag{47}$$

$$\cos\theta_z = \cos\delta * \cos\varphi * \cos\omega + \sin\delta * \sin\varphi \tag{48}$$

where θ it is the angle of the zenith of the sun's position concerning the north–south axis.

## 3.3 Initial and boundary conditions

To start up the analysis with a mathematical model of solar water collector required the initial boundary conditions for the various parameters, such as the water temperature at the entrance to the solar collector ($T_{w,sci}$), the glass cover (Tg), the ambient air ($T_a$) and the wind velocity ($V_a$). Knowing the number of days (n),

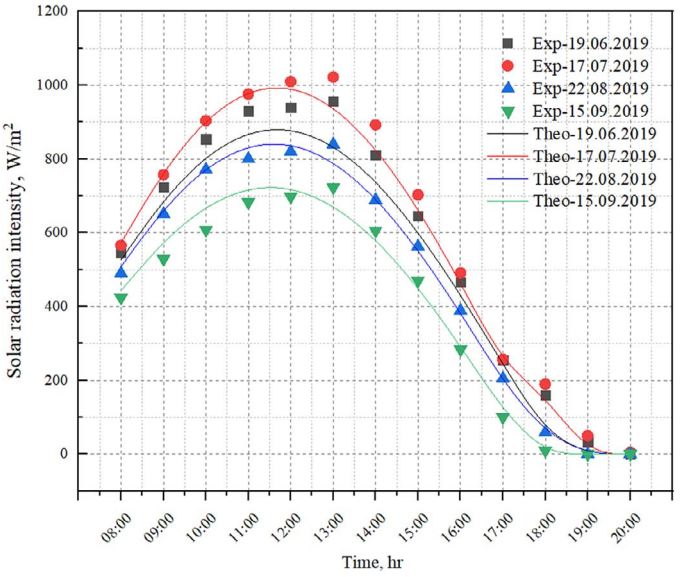


**Figure 5.** *The hourly change in solar radiation intensity for theoretical model and experimental results of the typical days: 19 June, 17 July, 22 August and 15 September of 2019.*

weather conditions, geometry, angle of collector tilt ($\beta$), operational data, initial conditions, the ambient air temperature ($T_a$) and the wind velocity ($V_a$).

## 4 RESULTS AND DISCUSSION

The theoretical model was validated using the corresponding experimental recorded results obtained during this study. The experimental defined design, operation and metrological parameters were used for the theoretical simulation. The study results illustrated the comparison of theoretical and experimental solar radiation intensity on solar water collectors which inclined 35°, the water temperature at the inlet and outlet of the solar collector, useful energy and thermal efficiency. The results of the proposed theoretical model in the current study showed good agreement with the data and results of the experimental work with a discrepancy of 4.7%. These deviations between experimental and theoretical results may result because the weather conditions, in the theoretical model, were considered constant. Also, these results showed consistency with standard parameters curves in other literature such as thermal efficiency. So, the proposed mathematical program proved reliable in understanding the thermal behavior of the flat plate SWH.

From the obtained results, it is found that all investigated parameters of the solar collector for four months were dependent on weather conditions; thus, the highest values were in July and the lowest is in October. The intensity of solar radiation is one of the most important weather parameters affecting the thermal performance of a solar collector. Figure 5 shows the hourly solar radiation intensity for experimental results and theoretical model, and four typical days were selected (19 June, 17 July, 22 August and 15 September) of 2019; all tests started at 8:00 am and ended at 8:00 pm. The values of the solar radiation intensity differed during the days of the test. The intensity of solar radiation increased after 8:00 am, and the highest value was recorded between 12:00 nn and 1:00 pm, to record 957, 1022, 840 and 723 W/m$^2$ for experimental results, and about 840, 946, 796 and 677 W/m$^2$ for the theoretical model of the typical 4 days (19 June, 17 July, 22 August and 15 September) of 2019. After midday, the solar radiation decreases to the lowest value at 8:00 pm.

Figure 6a and b shows the hourly variation of water temperatures at the inlet and outlet of the solar water collector for the four typical days (19 June, 17 July, 22 August and 15 September) of 2019. These temperatures are directly affected by the weather conditions, especially the intensity of solar radiation and ambient air temperature. As the intensity of solar radiation increased, the water temperature at the inlet and outlet of the solar collector increased. Therefore, at 2:00 pm, the temperature of the inlet water was recorded around 57.2 and 64.4°C experimentally and 60°C and 66.8°C theoretically on 19 June and 17 July 2019. While recorded on 22 August and 15 September of 2019, about 52.4°C and 49°C experimentally, 52.9°C and 49.2°C theoretically at 1:00 pm. Then the temperature of the water entering the collector decreases with the decrease in solar radiation after 2:00 pm, as shown in Figure 6a.

The same phenomenon was observed for the water temperature at the outlet of the solar collector, which was ∼62.8°C and 71°Cfor the experimental results and 63.5°C and 71.38°Cfor the theoretical model on 19 June and 17 July of 2019 at 2:00 pm. While recorded on 22 August and 15 September of 2019, ∼57.4°C and 53.2°C for experimental results, 57°C and 52.2°C for the theoretical model at 1:00 pm, respectively. After 2:00 pm, the solar radiation intensity begins to decrease. Then the temperature of the water leaving the collector decreases with decreasing solar radiation after 2:00 pm, as shown in Figure 6b.

Figure 7 shows the hourly variation of the useful energy gained from a solar water collector for the four typical days. From this figure, it is evident that at its highest solar radiation intensity around midday, the maximum value of the useful energy gained was recorded. Therefore, in the morning and after 2:00 pm, the solar radiation intensity values were relatively low; hence, the useful energy was relatively low. The highest values of useful energy gained were recorded on 17 July, which was 669.4 and 562.6 W for experimental results and theoretical model, respectively. However, lower thermal energy was gained on 19 June by 527.9 and 444.2 W, on 22 August by 418.2 and 365.9 W and on 15 September by 356.3 and 272.7 W for experimental results and theoretical model, respectively. This difference is due to the higher intensity of solar radiation on 17 July of 2019, compared with other months, and the greater difference in water temperatures between the inlet and outlet of the solar collector. Therefore, the useful energy gained on 17 July was greater than on other months.

Figure 8 shows the variance in the hourly thermal efficiency of a solar water collector. The hourly thermal efficiency of the flat plate solar water collector for all month's ranges between 33% and 66%, and the highest thermal efficiency recorded was on 17

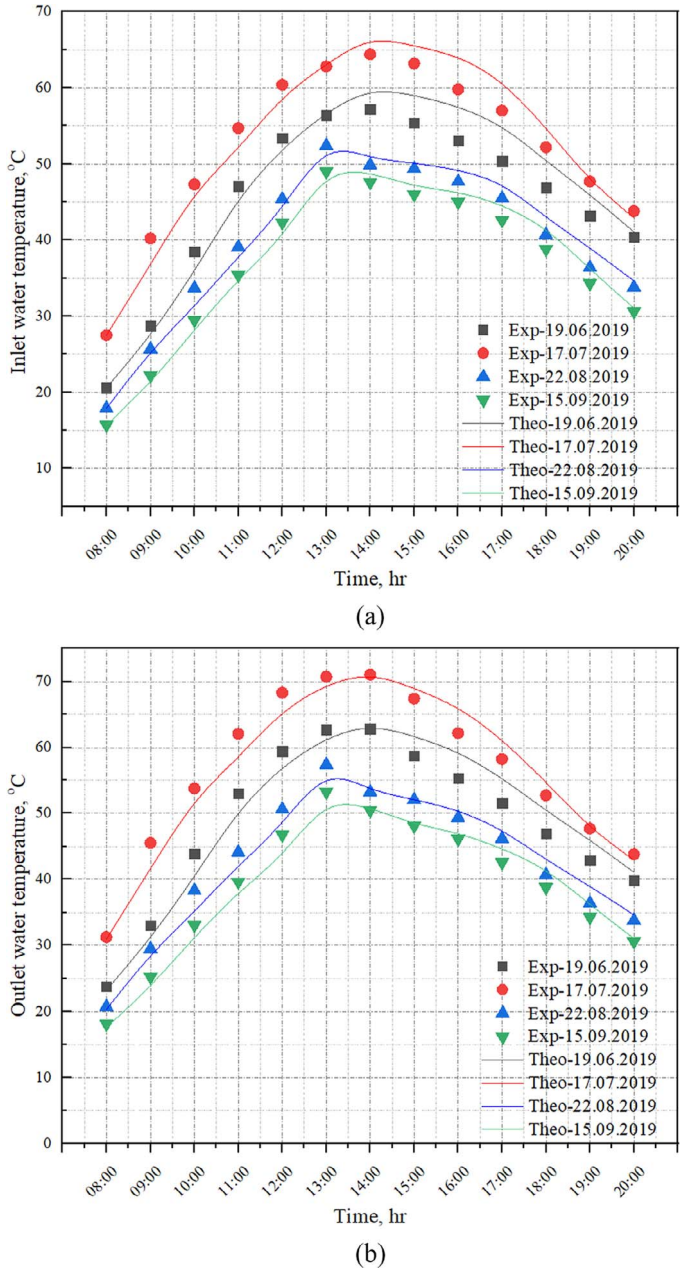


**Figure 6.** *The hourly change in water temperature for theoretical model and experimental results of the typical days: 19 June, 17 July, 22 August and 15 September of 2019; (a) at the inlet of the water collector; (b) at the outlet of the water collector.*

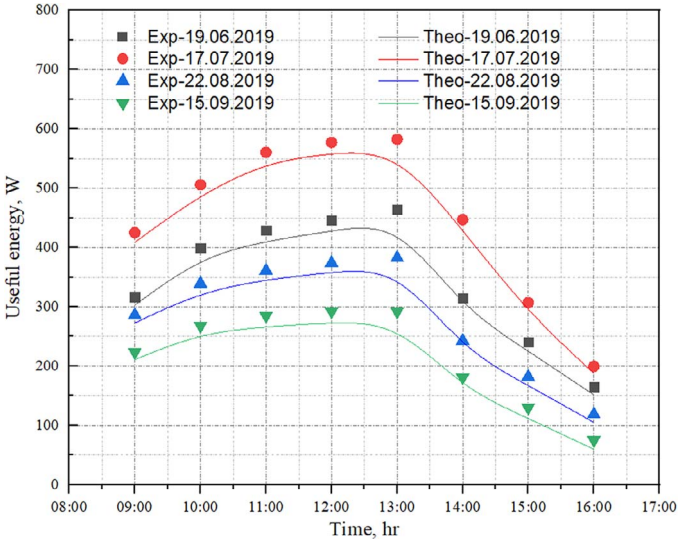


**Figure 7.** *Hourly variation in useful energy for theoretical model and experimental results for the four typical days.*

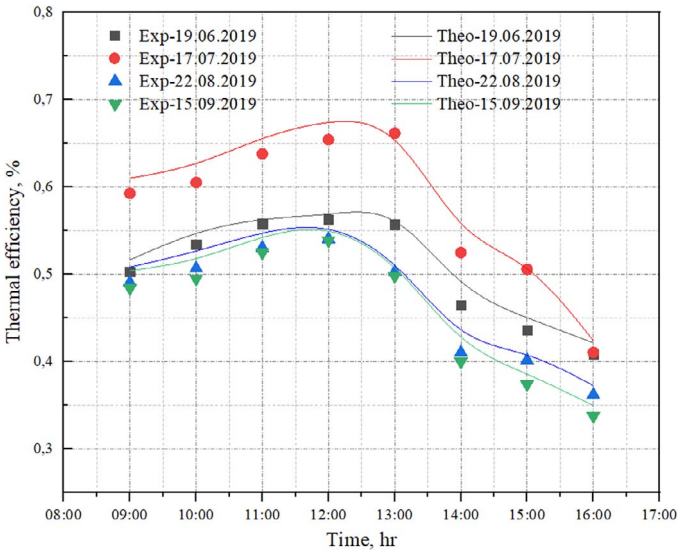


**Figure 8.** *Variation in thermal efficiency for theoretical model and experimental results for the four typical days.*

July 2019, due to the higher solar radiation intensity and useful energy gained on 17 July of 2019 compared with the other three typical days.

Table 2 listed the thermal efficiency of solar water collectors with a different design for previous studies in different climatic conditions. Good agreement has been obtained with the current solar water collector in terms of thermal efficiency in climatic conditions in Yekaterinburg, Russia, this means that the proposed mathematical program proved reliable in understanding the thermal behavior of the flat plate SWH.

## 5 CONCLUSION

In the current work, a theoretical and experimental investigation was conducted to evaluate the thermal performance of the flat plate SWH. Four months from June to September of 2019, and four typical days have been chosen in this study: 19 June, 17 July, 22 August and 15 September 2019, in climatic conditions in Yekaterinburg, Russia, and the following conclusion have been concluded.

**Table 2.** *Comparison of thermal efficiency of a current solar collector with previous studies.*

| The studies | Type of study | Type solar water collector, ($m^2$) | Flow rate, $L$/min | Thermal efficiency, % |
|---|---|---|---|---|
| [33], Iraq | Experimental | Flat plate collector surface lies a coiled tube, (1.4 $m^2$) | 5.3 − 6.51 | 40% to 60% |
| [34], Malaysia | Theoretical and experimental | Flat plate solar heater using a monolayer graphene nanofluids, (1 $m^2$) | 1.5 | 76.13% to 79.2% |
| [35], Iraq | Theoretical and experimental | Flat plate solar water collector, (1$m^2$) | 0.03 | 82% |
| The current study, Russia | Theoretical and experimental | Flat plate SWH type with 30 copper tubes (0.99$m^2$) | 1.2 | 41% to 66% (experimental)<br>42% to 67% (theoretical) |

1. There is a simultaneous increase in the water temperature and the intensity of solar radiation. During the four typical days, the highest water temperatures of the solar collector were recorded in midday by ∼57.2°C, 64.4°C, 52.4°C and 49°C at the inlet, and 62.8°C, 71°C, 57.4°C and 53.2°C at the outlet, while the solar radiation intensity recorded by about 957, 1022, 840 and 723 W/$m^2$ 19 June, 17 July, 22 August and 15 September 2019, respectively.
2. The highest rate of useful energy for the 4 months has been recorded at midday with the highest intensity of solar radiation. After 2:00 pm, the inlet and outlet water temperatures decreased due to the decrease in solar radiation intensity and thus the rate of useful energy gained decreased.
3. The highest values of useful energy gained were recorded on 17 July, which was 669.4 and 562.6 W for experimental results and theoretical model, respectively. However, lower thermal energy was gained on 19 June by 527.9 and 444.2 W, on 22 August by 418.2 and 365.9 W and on 15 September by 356.3 and 272.7 W for experimental results and theoretical model, respectively.
4. The thermal efficiency for four months ranged between 33% and 66%, and the highest was obtained on 17 July 2019, in which the higher solar radiation intensity was recorded.
5. The theoretical model results showed good agreement with the experimental work data. The same trend shows the average 4.7% deviation adopted for measurement in the experimental data and standard parameters curves in other literature such as thermal efficiency. So, the proposed mathematical program proved reliable in understanding the thermal behavior of the flat plate SWH.

## REFERENCES


[1] Molamohamadi Z, Talaei M. Analysis of a proper strategy for solar energy deployment in Iran using SWOT matrix. *Renew Energ Res Appl* 2022;**3**:71–8.

[2] Alayi R, Zishan F, Mohkam M *et al.* A sustainable energy distribution configuration for microgrids integrated to the national grid using back-to-back converters in a renewable power system. *Electronics* 2021;**10**:1826.

[3] Alayi R, Rouhi H. Techno-economic analysis of electrical energy generation from urban waste in Hamadan, Iran. *Int J Des Nature Ecodyn* 2020;**15**:337–41.

[4] Wahab A, Hassan A, Arslan Qasim M *et al.* Solar energy systems—potential of nanofluids. *J Mol Liq* 2019;**289**:111049.

[5] Shamshirgaran SR, Al-Kayiem HH, Sharma KV *et al.* State of the art of techno-economics of nanofluid-laden flat-plate solar collectors for sustainable accomplishment. *Sustain* 2020;**12**:1–42.

[6] Alayi R, Kumar R, Seydnouri SR *et al.* Energy, environment and economic analyses of a parabolic trough concentrating photovoltaic/thermal system. *Int J Low-Carbon Technol* 2021;**16**:570–6.

[7] Alayi R, Mohkam M, Seyednouri SR *et al.* Energy/economic analysis and optimization of on-grid photovoltaic system using CPSO algorithm. *Sustainability* 2021;**13**:12420.

[8] Sadeghi G, Nazari S, Ameri M *et al.* Energy and exergy evaluation of the evacuated tube solar collector using Cu2O/water nanofluid utilizing ANN methods. *Sustain Energy Technol Assess* 2020;**37**:100578.

[9] Muthuraman U, Shankar R, Kumar Nassa V *et al.* Energy and economic analysis of curved, straight, and spiral flow flat-plate solar water collector. *Int J Photoenergy* 2021;**2021**:5547274, 11 pages.

[10] Shateri A, Pishkar I, Mohammad BS. Optimization of heat transfer in an enclosure with a Trombe Wall and solar chimney. *Renew Energ Res Appl* 2022;**3**:103–14.

[11] Alayi R, Zishan F, Seyednouri SR *et al.* Optimal load frequency control of island microgrids via a PID controller in the presence of wind turbine and PV. *Sustainability* 2021;**13**:10728.

[12] Sampathkumar K, Arjunan TV, Senthilkumar P. Single basin solar still coupled with evacuated tubes—thermal modeling and experimental validation. *Int Energy J* 2011;**12**:53–66.

[13] Farahat M, Mousa M, Mahmoud N. Solar distiller with flat plate collector and thermal storage. *Int Conf Appl Mech Mech Eng* 2016;**17**:1–11.

[14] Mirmanto IMA, Sayoga AT, Wijayanta AP *et al.* Aziz, enhancement of continuous-feed low-cost solar distiller: effects of various fin designs. *Energies* 2021;**14**:4844.

[15] Shah SFA. 2017. Desalination of water: design, fabrication and performance evaluation of active solar still coupled with solar collector. In *1st International Conference on*, p. 16.

[16] Singh BP. Performance evaluation of a integrated single slope solar still with solar water heater. *Int J Mech Eng* 2011;**1**:67–70.

[17] Selimli S, Recebli Z, Ulker S. Solar vacuum tube integrated seawater distillation—an experimental study. *Facta Univ Ser Mech Eng* 2016;**14**:113–20.

[18] Sethi AK, Dwivedi VK. Exergy analysis of double slope active solar still under forced circulation mode. *Desalin Water Treat* 2013;**51**:7394–400.

[19] Mousa H, Abu-Arabi M, Al-Naerat M *et al.* Solar desalination indirect heating. *Int J Sustain Water Environ Syst* 2010;**1**:29–32.

[20] Alwan NT, Shcheklein SE, Ali OM. 2020. *Productivity of Enhanced Solar Still under Various Environmental Conditions in Yekaterinburg City / Russia*. IOP Conf. Ser. Mater. Sci. Eng., Institute of Physics Publishing.

[21] Alwan NT, Shcheklein SE, Ali OM. A practical study of a rectangular basin solar distillation with single slope using paraffin wax (PCM) cells. *Int J Energy Convers* 2019;**7**:162–70.

[22] Boumaaraf H, Boumaaraf B, Slimani ME *et al.* A comparative study on two different configurations of hybrid photovoltaic thermal collector with

experimental validation and uncertainty analysis. *Environ Prog Sustain Energy* 2022;**41**:e13704.
[23] Harrabi I, Hamdi M, Hazami M. Assessment of uncertainties in energetic and exergetic performances of a flat plate solar water heater. *Math Probl Eng* 2020;**2020**:1–12.
[24] Duffie JA, Beckman WA. 2013. *Solar Engineering of Thermal Processes*. Wiley.
[25] Bejan A. 1995. *Heat Transfer* 2nd edn. Wiley Interscience.
[26] Medugu DW, Ndatuwong L. Theoretical analysis of water distillation using solar still. *Phys Sci Int J* 2009;**4**:705–12.
[27] Fallis A. Metode penelitian Nursalam. *J Chem Inf Model* 2013;**53**:1689–99.
[28] Tarik S, Abdul-Ghafour Q, Ismael L. Study of transient simulation for solar heating system. 2011;**29**:677–97.
[29] Frid SE, Popel OS, Lisitskaya NV *et al.* Generalized clearness index frequency curves for the Russian Federation. *Dokl Phys* 2017;**62**: 278–80.
[30] Frid SE, Lisitskaya NV, Popel OS. Cumulative clearness index frequency distributions on the territory of the Russian Federation. *Dokl Phys* 2018;**63**:89–92.
[31] Benghanem M. Optimization of tilt angle for solar panel: case study for Madinah. *Saudi Arabia Appl Energy* 2011;**88**:1427–33.
[32] Al-Ani RR, Hameed A, Jawad M *et al.* Assessment of water quality in the selected sites on the Tigris River, Baghdad-Iraq. *Int J Adv Res* 2014;**2**:1125–31.
[33] Hashim WM, Shomran AT, Jurmut HA *et al.* Case study on solar water heating for flat plate collector. *Case Stud Therm Eng* 2018;**12**:666–71.
[34] Alawi OA, Kamar HM, Mallah AR *et al.* Experimental and theoretical analysis of energy efficiency in a flat plate solar collector using monolayer graphene nanofluids. *Sustainability* 2021;**13**:5416.
[35] Al-Saiydee MAM. Experimental and theoretical analysis of thermal losses in a flat plate solar heater with multi risers and headers. *J Mech Eng Res Dev* 2021;**44**:44–51.